Numerical study on a designable linear-resonant multiband single-layer fractal frequency-selective surface

Zhangqi Liao, Tao Wang, Yan Nie, Xian Wang, and Rongzhou Gong
Department of Electronic of Science and Technology, Huazhong University of Science and Technology, Wuhan 430074, People's Republic of China

(Received 11 April 2010; revised manuscript received 31 May 2010; published 20 July 2010)

In this paper, the multiband transmission resonant properties of single-layer Minkowski fractal planar frequency-selective surfaces (FSSs) at normal-incidence case were numerically investigated in detail. The self-similar iterative transformational method was proposed to construct the fractal FSSs. Both the finite integration technology and finite element method were used to calculate the magnitudes and phases of transmittances, and then the induced surface current and magnetic energy density distributions were demonstrated to analyze the insight physical picture of the multiband resonant feature. The results indicate that the individual resonant frequencies of our fractal FSSs present a periodical linear-resonant phenomenon and they could be designed easily and precisely just according to the geometrical characteristic of each iteration. With the intriguing resonant properties, the fractal FSS has a potential application in the fields of dual-band or multiband resonance.

DOI: 10.1103/PhysRevE.82.016603 PACS number(s): 41.20.Jb, 78.20.Ci, 78.66.Sq, 42.25.Bs

I. INTRODUCTION

With an ever-growing demand of antennas in both the military and the commercial sectors, a variety of approaches need to be developed to possess the highly desirable attributes including compact size, low profile, conformal, and multiband or broadband. Frequency-selective surface (FSS), a two-dimensional planar metallic periodic structure exhibiting the passband or stop-band properties, has been introduced into the field of antennas [1–8]. However, traditional FSS antennas become highly inefficient when the size is made much smaller than the operating wavelength and they are hard to realize multiband attribute [9]. Recently, the possibility of proposing the fractal FSSs to meet the demands of antennas, especially the multiband (primarily, dual band), has attracted a lot of attention [10–20].

The term *fractal*, involving broken or irregular fragments, was first coined by Mandelbrot [21] to describe a family of complex shapes that possess an inherent self-similarity or self-affinity in their geometrical structure. Fractal shapes, usually starting from simple geometries, can be created using iterative transformational methodology, including copying, scaling, and translation. The resonant frequencies of multiband presented by fractal FSSs could be determined by the self-similar iterative geometrical characteristics [22], which make it easy and controllable to design the multiband antennas.

In this paper, the Minkowski (MSK) loop fractal, of which the iterative methodology is simple with respect to other fractals, i.e., Koch curve and Sierpinski carpet [23], was chosen to discuss the electromagnetic periodical multiband resonant features in detail. By using the numerical methods of finite integration technology (FIT) and finite element method (FEM), the transmission properties were calculated and meanwhile the distributions of the induced surface currents and magnetic energy densities were demonstrated to get an insight of the physical picture of the resonances much more clearly. Then the relationship among individual resonant frequencies of fractal FSSs was analyzed and summarized. This paper expounds the entire process for the schema construction and the multiband resonant frequency design of Minkowski fractal FSSs.

II. STRUCTURE MODEL

The MSK loop fractal FSS could be obtained after a self-similar iterative growing procedure which is shown in Fig. 1, where the 0.02-mm-thick aluminum is printed on one side of 0.3-mm-thick FR-4 substrate (relative dielectric constant $\varepsilon_r=4.9$), with dimensions as follows: $L_1=4$ mm [Fig. 1(a)]; $L_2=8$ mm, $G_1=3$ mm, $D_1=D_2=2$ mm [Fig. 1(b)]; and $L_3=18$ mm, $G_2=6$ mm, $D_3=0.5$ mm, $D_4=D_5=D_6=2$ mm [Fig. 1(c)]. Particularly, all the MSK0, MSK1, and MSK2 loops have the same periodic dimension $P=20$ mm, and the same linewidth $W=0.2$ mm. In theory, the real fractal FSS is generated after infinite times of iterations; however, the fractal FSS with finite iterative times can meet the practical demands. Here, we choose two times of iterations. The constructing procedure for single-layer fractal FSS origins from

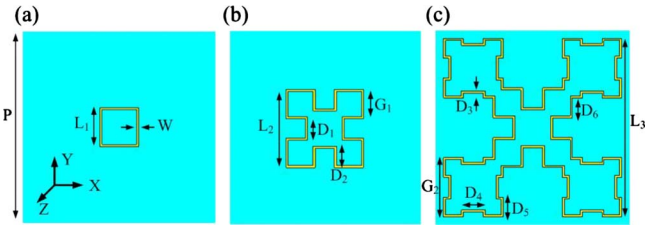

FIG. 1. (Color online) Self-similar iterative growing procedure of proposed MSK loop fractal FSSs: (a) stage 0: MSK0; (b) stage 1: MSK1; (c) stage 2: MSK2.

a simple square loop [Fig. 1(a), MSK0] and the next step to construct MSK1 in the process is to copy four self-similar loops to the four corners of MSK0, respectively [Fig. 1(b)]. This process is then repeated in order to get the MSK2 which is shown in Fig. 1(c). Each iteration involves transformations of scaling and translating the previous iteration. The resulting points of the geometry could be expressed as follows:

$$\text{previous points:} \quad p_i = (x_i, y_i),$$

$$\text{transformational formula:} \quad T_{1,2,3,4}(p_i) = \left[x_i \pm \left(\tfrac{3}{2}|x_i| - 1\right), y_i \pm \left(\tfrac{3}{2}|y_i| - 1\right)\right],$$

$$\text{resulting points:} \quad p_{i+1} = p_i \cup T_1(p_i) \cup T_2(p_i) \cup T_3(p_i) \cup T_4(p_i),$$

where p_{i+1}, the resulting set of points for the $i+1$ iteration, is composed of the union of the previous iteration points p_i and the transformed points T_1 through T_4.

III. NUMERICAL ANALYSIS

In our study, the propagating direction of incident electromagnetic wave (k) is along the negative Z axis ($k \| -z$), and meanwhile the electric and magnetic fields are parallel to the y ($E \| y$) and x ($H \| x$) directions, respectively, with x, y, and z as show in Fig. 1. For the fractal FSSs MSK0, MSK1, and MSK2, the transmission properties at normal-incidence case are numerically investigated using FIT method and FEM, with Floquet input-output port and master-slave boundary condition. The calculated results, including magnitudes and phases, are presented as followed in the left and right rows of Fig. 2, respectively. The differences of the calculated results between two methods may be caused by the fact that the FIT and FEM are both approximate solutions, with different solving procedures, mesh divisions, and other internal treatments. Although the different approximate solutions will bring in differences, however, the precision of the results matches our real requirements. In Fig. 2(a), MSK0 has one resonant frequency $f_1 = 14$ GHz. After the iteration procedures mentioned above, the circumferences of MSK1 and MSK2 are 48 and 144 mm, which are three and nine times longer than the case of MSK0 (circumference of 16 mm), respectively. According to Munk's theory [24], the wavelength of excitation is approximately equal to the circumference of the corresponding loop. Therefore, the resonant frequencies of MSK1 and MSK2 could be predicted to shift down to 4.67 and 1.56 GHz, which are 1/3 and 1/9 with respect to the case of MSK0, respectively. The calculated resonant frequencies f_1 in Figs. 2(b) and 2(c) are 7.1 and 2.2 GHz, and this basically agrees with our prediction. Apart from f_1, MSK1 has another one resonant frequency $f_2 = 13.4$ GHz, almost the same as the resonant frequency f_1 of MSK0; and, meanwhile, MSK2 has another two resonant frequencies $f_2 = 6.1$ GHz and $f_3 = 10.5$ GHz, nearly equal to f_1 and f_2 of MSK1. Both the magnitude and phase results show that each iteration could keep the former resonant frequencies of previous iteration almost unchanged and at the same time make out one additional controllably resonant frequency, determined by the geometrical characteristic of each iteration.

In order to get an insight into the physical picture of the intriguing individual resonant frequencies of MSK0, MSK1, and MSK2, the induced surface current distributions [25–27] were calculated, as shown in Fig. 3. As a result of the axisymmetric feature of the geometrical schemas, the current distributions are symmetrically placed, making it satisfied to analyze the left halves of MSK0, MSK1, and MSK2, called

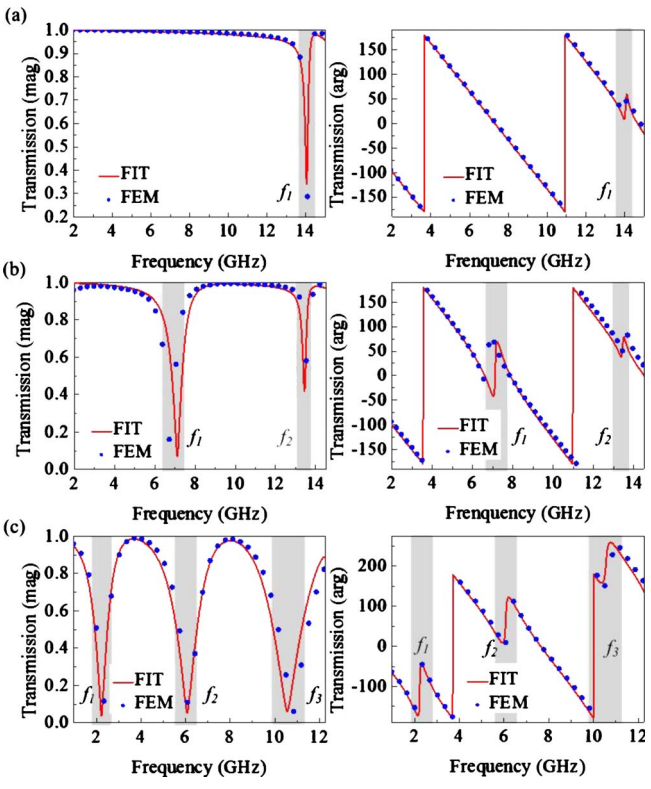

FIG. 2. (Color online) The left and right rows show the simulated magnitudes and phases of transmission properties at normal-incidence case, respectively: (a) MSK0, (b) MSK1, and (c) MSK2. Red solid lines and blue solid circles represent the calculated results using FIT method and FEM, respectively. The gray boxes indicate the individual resonant areas.

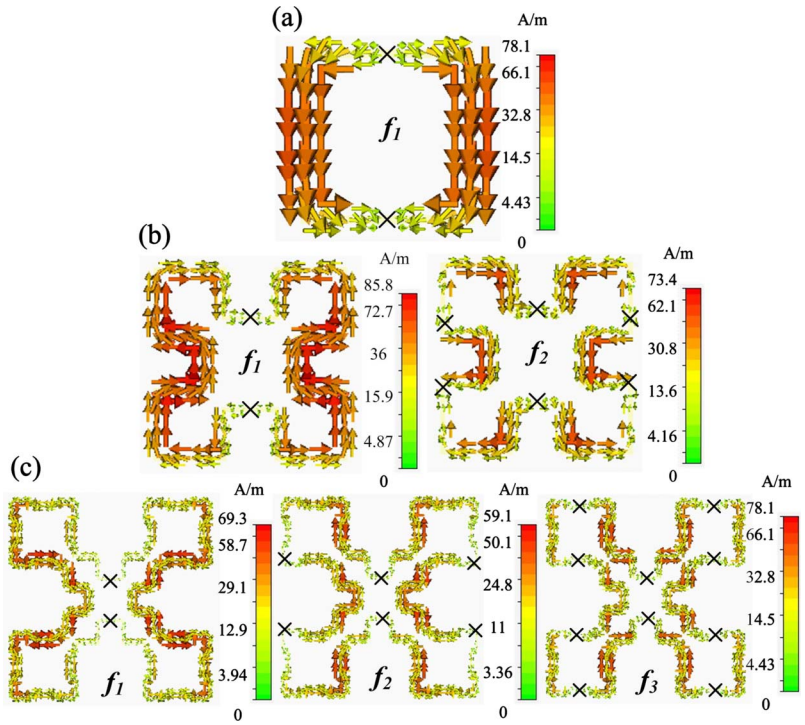

FIG. 3. (Color online) Surface current distributions of (a) MSK0, (b) MSK1, and (c) MSK2 at their resonant frequencies: (a) f_1=14 GHz; (b) f_1=7.1 GHz, f_2=13.4 GHz; and (c) f_1=2.2 GHz, f_2=6.1 GHz, f_3=10.5 GHz. The symbol "×" is on behalf of current null.

LH0, LH1, and LH2, correspondingly. For representing the geometrical lengths of LH0, LH1, and LH2, we define a ratio named L_{gs} $(s=0,1,2)$ here. The values of L_{g0}, L_{g1}, and L_{g2} are 8, 24, and 72 mm, respectively. For MSK0 [Fig. 3(a)], the current flows along the whole LH0 at the resonant frequency f_1 from one current null (marked by the symbol "×") to the other. Similarly, the current travels through the entire LH1 at the resonant frequency f_1 of MSK1 [Fig. 3(b)]. However, at the resonant frequency f_2 of MSK1, the current distribution is divided into three parts because of the appearance of two additional current nulls in LH1, varying differently from that of f_1 of MSK0. For MSK2 presented in Fig. 3(c), the current distributions at the resonant frequencies f_1 and f_2 are similar to the cases of f_1 and f_2 of MSK1, correspondingly. Remarkably, the current distribution of MSK2 at the resonant frequency f_3 is divided into five parts as a consequence of the existence of four current nulls in LH2. The results in Fig. 3 indicate that the current distributions could affect the resonant frequencies of each iteration in a special rule, which was further demonstrated in Fig. 4.

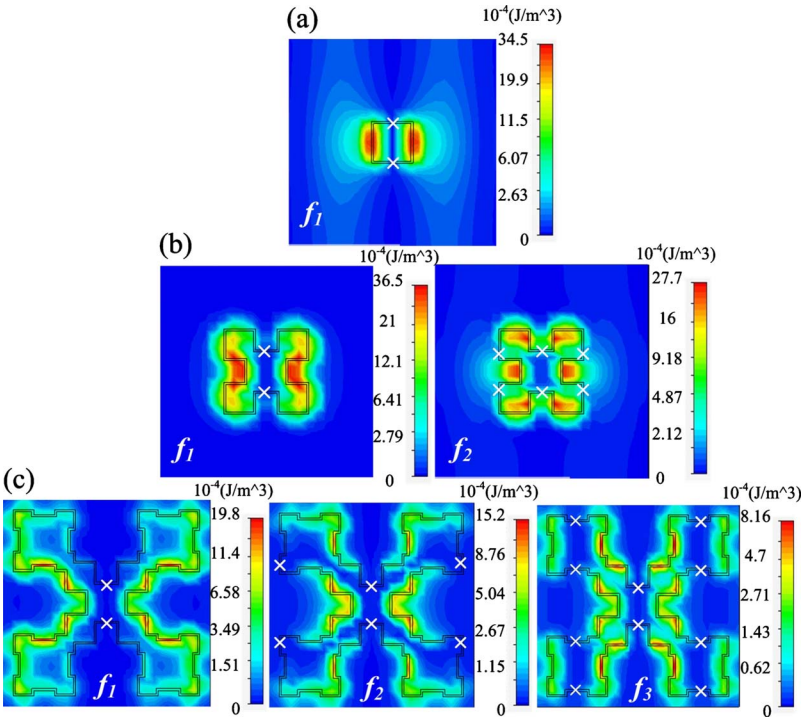

FIG. 4. (Color online) Magnetic energy density distributions of (a) MSK0, (b) MSK1, and (c) MSK2 at their resonant frequencies, corresponding to the surface current distribution results as shown in Fig. 3.

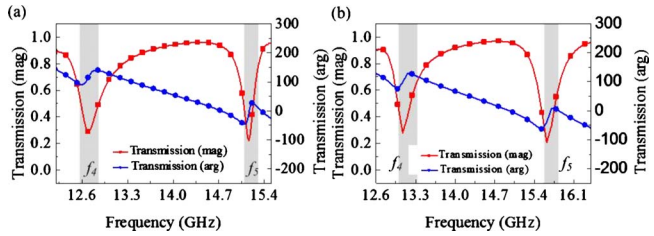

FIG. 5. (Color online) Simultaneous magnitudes (red solid squares) and phases (blue solid circles) of MSK2 transmission properties at normal-incidence case between 12 and 17 GHz using (a) FIT method and (b) FEM: f_4=13.1 GHz and f_5=15.3 GHz.

The former research on Salisbury screen [28,29] has pointed out that the resonant frequencies appear periodically when the thickness of dielectric substrate approaches a quarter of the resonant wavelength ($\lambda/4$) proportionally. Guided from the resonant phenomenon of Salisbury screen, the resonant frequencies of fractal FSSs are probably generated in period, too. Figure 4 shows the magnetic energy density distributions, which could present the corresponding effective dominant resonant areas of the surface currents in Fig. 3. Here, we define another ratio L_r for demonstrating the lengths of effective dominant resonant areas between two neighboring current nulls of fractal FSS, which is marked by the symbol "×." Significantly, LH1 and LH2 are cut into different sections with the increasing numbers of current nulls. Also we define a ratio R_{ep} for illustrating the effective dominant resonant proportions, by the formula $R_{ep}=L_{gs}/L_r$ ($s=0,1,2$). For MSK1, the proportion of f_2/f_1 is 1.89, differing from the R_{ep} value of 3. With the increasing numbers of iterative times, the proportions of f_i/f_1 ($i=2,3$) for MSK2 are nearly 2.77 and 4.77, which are close to the corresponding R_{ep} values of 3 and 5, with LH2 divided into three and five average parts, respectively. It seems that the resonant frequencies are inverse of the corresponding values of L_r. Therefore, MSK2 could be predicted to have another resonant frequency at 15.4 GHz (seven times of f_1) where LH2 is divided into seven average parts with six current nulls.

The transmission properties of MSK2 within the frequency band of 12–17 GHz were calculated as shown in Fig. 5. Significantly, there appears a resonant frequency f_5 around 15.3 GHz, agreeing well with the predicted resonant frequency of 15.4 GHz. The surface current and magnetic energy distributions in Fig. 6(a) demonstrate clearly that LH2 is cut into seven sections with average length because of the existence of the six current nulls ($R_{ep}=7$), verifying our above prediction. Figure 5 shows that there is one unexpected frequency f_4 resonated at 13.1 GHz, six times of f_1. As analyzed before, LH2 is supposed to be divided into six pieces averagely and has five current nulls. However, considerably different in Fig. 6(b), the surface currents and magnetic energy densities are split into four parts with almost the same length, which distribute irregularly along LH2, compared with the case of f_5. As indicated in the dashed boxes in Fig. 6(b), the L_r value is 12.5 mm, nearly 1/6 of L_{g2} with $R_{ep}=5.76$. Figure 7(a) shows another resonant frequency f_6 appearing around 17.6 GHz of MSK2 (eight times of f_1), analyzed by the surface current and magnetic energy density distributions as shown in Figs. 7(b) and 7(c). Similarly to the case of f_4, the effective dominant resonant areas of LH2 are separated into two parts with nearly the same length and distributed irregularly at the resonant frequency f_6, with the passing length of the predominant current, 8.5 mm, exactly 1/8 of LH2 with $R_{ep}=8.47$. Although totally differing from each other, the current and magnetic energy density distributions at f_4, f_5, and f_6 all exhibit obviously that the resonant frequencies of the proposed fractal FSSs are indeed generated periodically and are inverse of the lengths of effective dominant resonant areas, as we conjectured before.

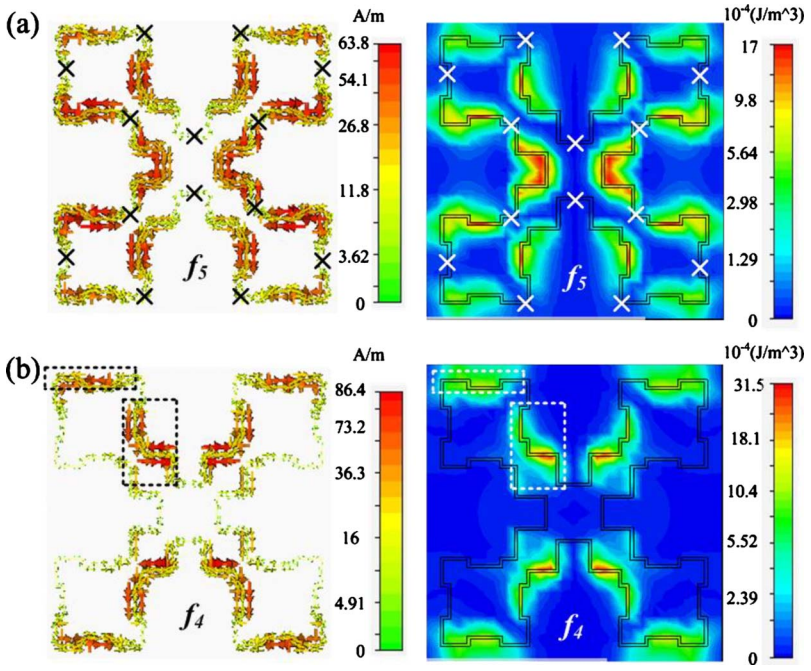

FIG. 6. (Color online) Surface current distributions (left row) and magnetic energy density distributions (right row) of MSK2 at resonant frequencies: (a) f_5=15.3 GHz and (b) f_4=13.1 GHz. The two black and two white dashed boxes as shown in (b) indicate a quarter of dominant resonant parts at the frequency f_4 in surface current and magnetic energy density distributions, respectively.

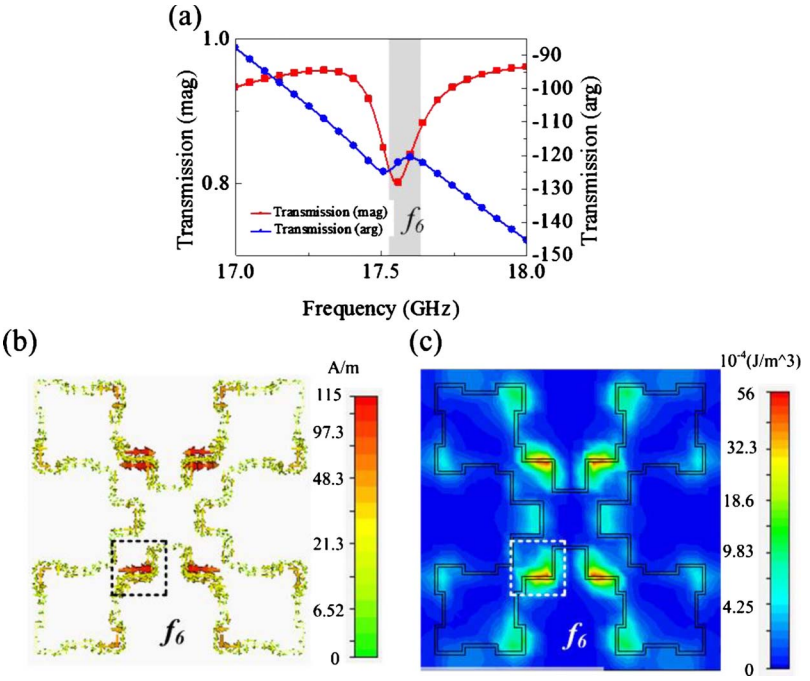

FIG. 7. (Color online) (a) Simultaneous magnitudes (red solid squares) and phases (blue solid circles) of MSK2 transmission properties at normal-incidence case in the 17–18 GHz frequency band; (b) surface current distribution at the frequency f_6=17.6 GHz; (c) magnetic energy density distribution at the frequency f_6.

As discussed above, our fractal FSS MSK2 could reveal the multiband feature, with individual resonant frequencies f_1=2.2 GHz, f_2=6.1 GHz, f_3=10.5 GHz, f_4=13.1 GHz, f_5=15.3 GHz, and f_6=17.6 GHz, respectively. The proportions of f_i/f_1 (i=1,2,3,4,5,6) obviously approach the R_{ep} values, illustrated in Table I. The relationship of the frequencies f_i (axis Y) versus the R_{ep} values (axis X) is further investigated as follows in Fig. 8. The discrete resonant points f_i, marked by red crosses, can be fitted to a curve, which is shown as the blue straight line. Intriguingly, the resonant frequencies of MSK2 appear in period and the relationship could be expressed by a linear formula $f_i=f_1R_{ep}$ (i=1,2,3,4,5,6). Taking advantage of this equation, the individual resonant frequencies of MSK2 could be predicted and controlled precisely at the fundamental of f_1, and meanwhile f_1 can be determined strictly according to the self-similar iterative geometrical characteristic. As a result, we could use the fractal FSSs to realize the dual-band and multiband resonant features easily and designably under different practical requirements.

TABLE I. Analysis on the individual resonant frequencies f_i (i=1,2,3,4,5,6) of MSK2.

	Frequency (GHz)	f_i/f_1	R_{ep} value
f_1	2.2	1.00	1
f_2	6.1	2.77	3
f_3	10.5	4.77	5
f_4	13.1	5.95	5.76
f_5	15.3	6.95	7
f_6	17.6	8.00	8.47

IV. CONCLUSION

In summary, the single-layer Minkowski fractal FSS constructed by self-similar iterative transformational method was studied using FIT and FEM numerical methodologies. This planar fractal FSS can exhibit a multiband behavior. Each iteration in finite times for our real demands could generate one additional resonant frequency that is determined by the geometrical characteristic and keep the former resonant frequencies of previous iterations almost unchanged at the same time. After n ($n\to\infty$) iterations, the fractal FSS will approach definite schema and thus the resonant properties will also converge to definite values. The magnitudes and phases of transmittances show that the resonant frequencies of our fractal FSS appear periodically. By demonstrating the induced surface current and magnetic energy density distributions, we learned about the physical insight picture more

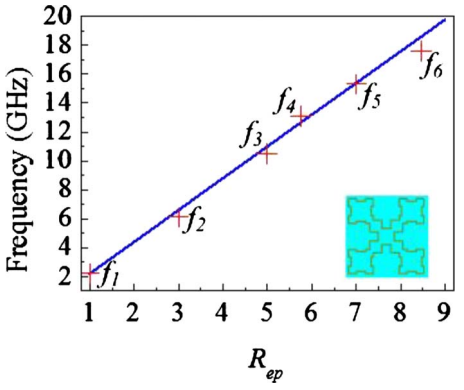

FIG. 8. (Color online) Relationship between the frequencies of characteristic resonant points (red cross) f_i (i=1,2,3,4,5,6) and the R_{ep} values of MSK2 loop.

clearly and it is found that the resonant frequencies are inverse of the following lengths of the corresponding effective dominant resonant areas. The multiband resonant frequencies reveal a kind of linear relationship with respect to the defined proportion R_{ep}. Taking advantage of this linearly fitting curve, the other resonant frequencies could be predicted and controlled precisely. In this paper, we illustrate a detailed design process for constructing the fractal FSS shapes and the multiband resonant frequencies, which could be helpful to meet the desirable attributes of antennas.

[1] D. F. Sievenpier, Ph.D. thesis, University of California–Los Angeles, 1999.

[2] F. Yang and Y. Rahmat-Samii, IEEE Trans. Antennas Propag. **51**, 2691 (2003).

[3] H. Mosallaei and K. Sarabandi, IEEE Trans. Antennas Propag. **52**, 2403 (2004).

[4] D. J. Kern, D. H. Werner, A. Monorchio, L. Lanuzza, and M. J. Wilhelm, IEEE Trans. Antennas Propag. **53**, 8 (2005).

[5] C. R. Simovski, P. de Maagt, and I. Melchakova, IEEE Trans. Antennas Propag. **53**, 908 (2005).

[6] R. W. Davies, I. L. Morrow, J. F. Cooper, and I. Youngs, Microwave Opt. Technol. Lett. **48**, 1022 (2006).

[7] A. Pirhadi, M. Hakkak, F. Keshmiri, and R. K. Baee, IEEE Trans. Antennas Propag. **55**, 1682 (2007).

[8] M. Hosseini and M. Hakkak, IEEE Antennas Wireless Propag. Lett. **7**, 58 (2008).

[9] C. P. Baliarda, J. Romeu, and A. Cardama, IEEE Trans. Antennas Propag. **48**, 1773 (2000).

[10] K. J. Vinoy, K. A. Jose, V. K. Varadan, and V. V. Varadan, Proc. SPIE **4334**, 176 (2001).

[11] W. J. Wen, L. Zhou, J. S. Li, W. K. Ge, C. T. Chan, and P. Sheng, Phys. Rev. Lett. **89**, 223901 (2002).

[12] C. Borja and J. Romeu, IEEE Trans. Antennas Propag. **51**, 1281 (2003).

[13] M. Ohira, H. Deguchi, M. Tsuji, and H. Shigesawa, IEEE Trans. Antennas Propag. **52**, 2925 (2004).

[14] M. J. Facchine and D. H. Werner, Electromagnetics **26**, 289 (2006).

[15] R. Holakouei, J. Nourinia, and C. Ghobadi, AEU, Int. J. Electron. Commun. **61**, 568 (2007).

[16] A. R. Chandran, M. Gopikrishna, C. K. Aanandan, P. Mohanan, and K. Vasudevan, PIER **69**, 323 (2007).

[17] J. C. Zhang, Y. Z. Yin, and J. P. Ma, PIER Lett. **8**, 1 (2009).

[18] R. M. S. Cruz, P. H. da F. Silva, and A. G. d'Assuncao, Microwave Opt. Technol. Lett. **51**, 3014 (2009).

[19] W. T. Wang, P. F. Zhang, S. X. Gong, B. Lu, J. Ling, and T. T. Wan, Microwave Opt. Technol. Lett. **51**, 2541 (2009).

[20] J. Y. Xue, S. X. Gong, P. F. Zhang, W. Wang, and F. F. Zhang, PIER Lett. **13**, 131 (2010).

[21] B. B. Mandelbrot, *The Fractal Geometry of Nature* (Freeman, New York, 1983).

[22] J. P. Gianvittorio, J. Romeu, S. Blanch, and Y. Rahmat-Samii, IEEE Trans. Antennas Propag. **51**, 3088 (2003).

[23] D. H. Werner and S. Ganguly, IEEE Antennas Propag. Mag. **45**, 38 (2003).

[24] B. A. Munk, *Frequency Selective Surfaces: Theory and Design* (Wiley, New York, 2000).

[25] P. Ding, E. J. Liang, L. Zhang, Q. Zhou, and Y. X. Yuan, Phys. Rev. E **79**, 016604 (2009).

[26] J. H. Lv, B. R. Yan, M. H. Liu, and X. W. Hu, Phys. Rev. E **80**, 026605 (2009).

[27] J. H. Lv, B. R. Yan, M. H. Liu, and X. W. Hu, Phys. Rev. E **79**, 017601 (2009).

[28] R. L. Fante and M. T. McCormack, IEEE Trans. Antennas Propag. **36**, 1443 (1988).

[29] D. J. Kern and D. H. Werner, Microwave Opt. Technol. Lett. **38**, 61 (2003).